ELSEVIER

Journal of Fluorine Chemistry 110 (2001) 89–107

JOURNAL OF FLUORINE CHEMISTRY

www.elsevier.com/locate/jfluchem

Structural and theoretical studies of $Xe(OChF_5)_2$ and $[XeOChF_5][AsF_6]$ (Ch = Se, Te)

Barbara A. Fir[a], Hélène P.A. Mercier[a], Jeremy C.P. Sanders[a], David A. Dixon[b], Gary J. Schrobilgen[a,*]

[a]*Department of Chemistry, McMaster University, Hamilton, ON L8S 4M1, Canada*
[b]*William R. Wiley Environmental Molecular Sciences Laboratory, Pacific Northwest National Laboratory, 906 Battelle Blvd., P.O. Box 999, KI-83 Richland, WA 99352, USA*

Received 28 February 2001; accepted 26 March 2001

Dedicated to our colleague Professor Karl O. Christe on the occasion of his 65th birthday and in appreciation of his long friendship and his many outstanding synthetic and structural contributions to the field of inorganic fluorine chemistry

Abstract

The $XeOSeF_5^+$ cation has been synthesized for the first time and characterized in solution by ^{19}F, ^{77}Se and ^{129}Xe NMR spectroscopy and in the solid state by X-ray crystallography and Raman spectroscopy with AsF_6^- as its counter anion. The X-ray crystal structures of the tellurium analogue and of the $Xe(OChF_5)_2$ derivatives have also been determined: $[XeOChF_5][AsF_6]$ crystallize in tetragonal systems, $P4/n$, $a = 6.1356(1)$ Å, $c = 13.8232(2)$ Å, $V = 520.383(14)$ Å^3, $Z = 2$ and $R_1 = 0.0453$ at -60°C (Te) and $a = 6.1195(7)$ Å, $c = 13.0315(2)$ Å, $V = 488.01(8)$ Å^3, $Z = 2$ and $R_1 = 0.0730$ at -113°C (Se); $Xe(OTeF_5)_2$ crystallizes in a monoclinic system, $P2_1/c$, $a = 10.289(2)$ Å, $b = 9.605(2)$ Å, $c = 10.478(2)$ Å, $\beta = 106.599(4)°$, $V = 992.3(3)$ Å^3, $Z = 4$ and $R_1 = 0.0680$ at -127°C; $Xe(OSeF_5)_2$ crystallizes in a triclinic system, $R\bar{3}$, $a = 8.3859(6)$ Å, $c = 12.0355(13)$ Å, $V = 732.98(11)$ Å^3, $Z = 3$ and $R_1 = 0.0504$ at -45°C. The energy minimized geometries and vibrational frequencies of the $XeOChF_5^+$ cations and $Xe(OChF_5)_2$ were calculated using density functional theory, allowing for definitive assignments of their experimental vibrational spectra.

Keywords: Xenon; Oxopentafluorotellurium(VI); Oxopentafluoroselenium(VI); X-ray crystallography; Density functional theory; Vibrational spectroscopy

1. Introduction

Xenon(II) derivatives of the highly electronegative $OTeF_5$ and $OSeF_5$ ligands have been extensively studied. The $OTeF_5$ and $OSeF_5$ groups have effective group electronegativities approaching that of fluorine and are capable of stabilizing essentially all of the same oxidation states as fluorine [1–3]. Consequently, nearly all of the chemistry of $OTeF_5$ and $OSeF_5$ compounds has been developed by analogy with that of the existing fluorides although that of the $OSeF_5$ group is less extensive [4,5].

The present work was undertaken to complete the characterization of the $[XeOChF_5][AsF_6]$ salts and of their related $Xe(OChF_5)_2$ derivatives. The $[XeOSeF_5][AsF_6]$ salt has been synthesized and characterized for the first time in both the solid state and solution, while $[XeOTeF_5][AsF_6]$ and $Xe(OChF_5)_2$ have been characterized by X-ray crystallography. Density functional theory (DFT) calculations were also performed on all compounds providing more complete assignments of their vibrational frequencies.

2. Results and discussion

2.1. Synthesis of $[XeOSeF_5][AsF_6]$

The compounds $Xe(OSeF_5)_2$ and $FXeOSeF_5$ were prepared in quantitative yield by reaction of SeO_2F_2 with XeF_2 as previously described [6], and the salt, $[XeOSeF_5][AsF_6]$, has been prepared by analogy with $[XeOTeF_5][AsF_6]$ [7] according to Eq. (1). Like the tellurium analogue,

$$FXeOSeF_5 + AsF_5 \rightarrow [XeOSeF_5][AsF_6] \quad (1)$$

$[XeOSeF_5][AsF_6]$ is a stable yellow solid at room temperature that readily sublimes under dynamic vacuum at 45°C. The $XeOSeF_5^+$ cation is resistant to solvolytic attack by BrF_5 at -51°C, although small amounts of SeF_6 (59.1 ppm, $^1J(^{19}F–^{77}Se)$, 1428 Hz) were detected after dissolution of

* Corresponding author. Tel.: +1-905-525-9140/ext. 23306; fax: +1-905-522-2509.
E-mail address: schrobil@mcmaster.ca (G.J. Schrobilgen).

0022-1139/01/$ – see front matter
PII: S0022-1139(01)00416-X

the sample in BrF_5 at or near −50°C. The $XeOTeF_5^+$ cation has been shown to rapidly solvolyze at room temperature forming TeF_6, and $XeF_2{\cdot}[BrOF_2][AsF_6]$ [8]. The ^{19}F NMR spectrum of the $OSeF_5$ group was significantly broadened at −51°C and likely arises from the chemical exchange processes represented by Eq. (2).

$$XeOSeF_5^+ + AsF_6^-(BrF_5) \rightleftharpoons FXeOSeF_5 + AsF_5(BrF_4^+) \quad (2)$$

2.2. ^{19}F, ^{77}Se and ^{129}Xe NMR spectra of $[XeOSeF_5][AsF_6]$

The ^{19}F NMR spectrum of $[XeOSeF_5][AsF_6]$ in SbF_5 solvent at 28°C (BrF_5 solvent, −51°C) consists of a first order AX_4 spectrum in the fluorine-on-selenium(VI) region of the spectrum and is accompanied by ^{77}Se ($I = 1/2$, 7.58%) satellites: $\delta(F_A)$, 57.1 [62.2] ppm; $\delta(F_X)$, 74.9 [73.3] ppm; $^2J(^{19}F_A–^{19}F_X)$, 216 [219] Hz; $^1J(^{19}F_A–^{77}Se)$, 1459 (not resolved owing to increased line broadening in BrF_5) Hz; $^1J(^{19}F_X–^{77}Se)$, 1415 [1398] Hz. The ^{77}Se NMR spectrum (SbF_5 solvent, 29°C) consists of a single ^{77}Se environment at 627.5 ppm, comprised of a binomial doublet of quintets resulting from the spin–spin couplings $^1J(^{19}F_A–^{77}Se) = 1460$ Hz and $^1J(^{19}F_X–^{77}Se) = 1415$ Hz. The ^{129}Xe spectrum in SbF_5 solvent at 25°C (BrF_5 solvent, −56°C) consists of a single resonance at −1349.0 [−1438] ppm in the xenon(II) region of the spectrum. In contrast with the ^{129}Xe spectrum of $XeOTeF_5^+$, the $^3J(^{129}Xe–^{19}F_e)$ coupling of $XeOSeF_5^+$ was not resolved and is likely the result of a greater field dependent shielding anisotropy in the selenium case arising from the significantly higher magnetic field (5.8719 T) used to record the ^{129}Xe spectrum of the $XeOSeF_5^+$ cation versus that used to record the ^{129}Xe NMR spectrum of $XeOTeF_5^+$ (2.1139 T) [8].

The ^{19}F chemical shifts of $XeOSeF_5^+$ are significantly deshielded with respect to those observed for $XeOTeF_5^+$ under similar conditions (F_A, −54.6 ppm and F_X, −41.0 ppm; SbF_5 solvent at 25°C) [8] although the frequency differences between F_A and F_X are comparable. The $^2J(^{19}F_A–^{19}F_X)$ coupling in $XeOSeF_5^+$ is greater than that in $XeOTeF_5^+$ (172.2 Hz). The ^{129}Xe chemical shift of $XeOSeF_5^+$ (−1349 ppm) is significantly deshielded with respect to that of the $XeOTeF_5^+$ cation under similar conditions ($\delta(^{129}Xe) = -1472$ ppm, SbF_5 solvent at 25°C) [8] and is consistent with the trend observed for a mixture of $Xe(OSeF_5)_2$ (−2200 ppm), $F_5TeOXeOSeF_5$ (−2289 ppm) and $Xe(OTeF_5)_2$ (−2379 ppm) recorded in $CFCl_3$ at room temperature [9]. This suggests that the effective electronegativity of the $OSeF_5$ group is somewhat greater than that of the $OTeF_5$ group.

The $^1J(^{19}F–^{77}Se)$ couplings are significantly less than the $^1J(^{19}F–^{125}Te)$ couplings ($^1J(^{19}F_A–^{125}Te)$, 3802 Hz and $^1J(^{19}F_X–^{125}Te)$, 3814 Hz). Removal of the nuclear dependencies and inclusion of a relativistic correction ($^1K(F–Se)_{RC}$ values are given in { }) yield reduced coupling constants [10,11], $^1K(F–Se)$ (F_A, 67.40 {58.36} and F_X, 65.37 {56.60} $\times 10^{20}$ NA^{-2} m^{-3}), which are also less than the $^1K(F–Te)$ values (F_A, 127.46 {88.58} and F_X, 127.86 {88.85}$\times$ 10^{20} NA^{-2} m^{-3}). The trend in reduced coupling constants is the same as that observed for SF_6, SeF_6 and TeF_6 [12].

2.3. X-ray crystal structures of $[XeOChF_5][AsF_6]$ and $Xe(OChF_5)_2$ (Ch = Te, Se)

A summary of the refinement results and other crystallographic information are given in Table 1. Important bond lengths and bond angles are listed in Table 2 along with the calculated values (see Section 2.5).

The crystal structures of $[XeOTeF_5][AsF_6]$ and $[XeOSeF_5][AsF_6]$ are reported for the first time. Both compounds are found to be isostructural and present the same four-fold orientational disorder of the fluorine and oxygen atoms (Fig. 1). The compound, $Xe(OSeF_5)_2$, had been previously studied by X-ray crystallography [13], but its room

Table 1
Summary of crystal data and refinement results for $[XeOTeF_5][AsF_6]$, $[XeOSeF_5][AsF_6]$, $Xe(OTeF_5)_2$, and $Xe(OSeF_5)_2$

	$[XeOTeF_5][AsF_6]$	$[XeOSeF_5][AsF_6]$	$Xe(OTeF_5)_2$	$Xe(OSeF_5)_2$
Empirical formula	$AsF_{11}OTeXe$	$AsF_{11}OSeXe$	$F_{10}O_2Te_2Xe$	$F_{10}O_2Se_2Xe$
Molecular weight (g mol^{-1})	558.82	510.18	608.50	511.22
T (°C)	−60	−113	−127	−45
λ (Å)	0.71073	0.71073	0.71073	0.71073
Space group (No.)	*P4/n*(85)	*P4/n*(85)	$P2_1/c$(14)	$R\bar{3}$(148)
a (Å)	6.1356(1)	6.1195(7)	10.289(2)	8.3859(6)
b (Å)	6.1356(1)	6.1195(7)	9.605(2)	8.3859(6)
c (Å)	13.8232(2)	13.0315(2)	10.478(2)	12.0355(13)
β (°)	90	90	106.599(4)	90
V (Å^3)	520.383(14)	488.01(8)	992.3(3)	732.98(11)
Z (molecules/unit cell)	2	2	4	3
Calculated density (g cm^{-3})	3.566	3.472	4.073	3.474
μ (mm^{-1})	9.347	10.766	9.368	11.108
R_1[a], wR_2[b] [$I > 2\sigma(I)$]	0.0453, 0.1345	0.0730, 0.1664	0.0680, 0.1589	0.0504, 0.1216

[a] R_1 is defined as $\sum ||F_o| - |F_c|| / \sum |F_o|$ for $I > 2\sigma(I)$.

[b] wR_2 is defined as $\left[\sum[w(F_o^2 - F_c^2)^2] / \sum w(F_o^2)^2\right]^{1/2}$ for $I > 2\sigma(I)$.

Table 2
Experimental geometries for $[XeOChF_5][AsF_6]$, and $Xe(OChF_5)_2$, and calculated geometries for $XeOChF_5^+$, and $Xe(OChF_5)_2$ (Ch = Se, Te)[a]

	Te		Se	
	Experimental	DFT[a]	Experimental	DFT[a]
$[XeOTeF_5][AsF_6]$ and $[XeOSeF_5][AsF_6]$				
Bond lengths (Å)				
Ch(1)–F(1)	1.80(2)	1.776	1.72(4)	1.627
Ch(1)–F(2)	1.81(2)	1.803	1.65(4)	1.668
Ch(1)–F(3)	1.82(2)	1.788	1.70(3)	1.646
Ch(1)–F(4)	1.84(2)	1.788	1.72(5)	1.646
Ch(1)–F(5)	1.79(3)	1.810	1.70(3)	1.670
Ch(1)–O(1)	1.85(3)	1.969	1.74(4)	1.845
As(1)–F(6)	1.72(2)		1.73(4)	
As(1)–F(7)	1.69(2)		1.69(2)	
As(1)–F(8)	1.74(2)		1.76(3)	
As(1)–F(9)	1.72(2)		1.71(2)	
As(1)–F(10)	1.72(2)		1.74(3)	
As(1)–F(11)	1.81(2)		1.80(4)	
Xe(1)–O(1)	1.96(4)	1.893	2.04(4)	1.902
Xe(1)–F(11)	2.24(3)		2.31(4)	
Bond angles (°)				
As(1)–F(11)–Xe(1)	135(1)		129(2)	
Ch(1)–O(1)–Xe(1)	128(2)	119.6	120(3)	118.3
O(1)–Ch(1)–F(1)	175(1)	178.4	171(3)	177.7
O(1)–Ch(1)–F(2)	93(2)	88.0	94(3)	89.5
O(1)–Ch(1)–F(3)	89(2)	87.0	94(3)	84.8
O(1)–Ch(1)–F(4)	93(2)	83.3	76(3)	85.1
O(1)–Ch(1)–F(5)	99(2)	88.0	92(3)	89.2
O(1)–Xe(1)–F(11)	174(1)		174(2)	
F(1)–Ch(1)–F(2)	92(2)	92.1	95(2)	92.3
F(1)–Ch(1)–F(3)	87(3)	92.8	76(2)	93.4
F(1)–Ch(1)–F(4)	85(4)	95.2	106(2)	93.5
F(1)–Ch(1)–F(5)	85(3)	93.6	87(2)	92.2
F(2)–Ch(1)–F(3)	165(3)	174.8	168(2)	174.2
F(2)–Ch(1)–F(4)	90(2)	90.9	72(2)	90.0
F(2)–Ch(1)–F(5)	67(2)	88.4	98(2)	88.8
F(3)–Ch(1)–F(4)	105(2)	90.3	102(2)	90.3
F(3)–Ch(1)–F(5)	98(3)	89.7	90(2)	90.2
F(4)–Ch(1)–F(5)	154(2)	171.3	164(3)	174.2
F(6)–As(1)–F(7)	89(4)		89(2)	
F(6)–As(1)–F(8)	101(2)		101(2)	
F(6)–As(1)–F(9)	91(5)		98(2)	
F(6)–As(1)–F(10)	86(3)		86(2)	
F(6)–As(1)–F(11)	175(3)		176(1)	
F(7)–As(1)–F(8)	85(1)		86(2)	
F(7)–As(1)–F(9)	176(2)		173(2)	
F(7)–As(1)–F(10)	96(3)		95(1)	
F(7)–As(1)–F(11)	96(2)		95(2)	
F(8)–As(1)–F(9)	99(2)		93(1)	
F(8)–As(1)–F(10)	172(2)		173(2)	
F(8)–As(1)–F(11)	81(2)		81(2)	
F(9)–As(1)–F(10)	80(4)		85(2)	
F(9)–As(1)–F(11)	84(2)		78(2)	
F(10)–As(1)–F(11)	91(3)		92(2)	
	Experimental			DFT
$Xe(OTeF_5)_2$				
Bond lengths (Å)				
Xe(1)–O(1)	2.119(11)	Xe(2)–O(2)	2.112(12)	1.996, 1.996
O(1)–Te(1)	1.843(11)	O(2)–Te(2)	1.842(11)	1.831, 1.831
Te(1)–F(1)	1.843(10)	Te(2)–F(6)	1.855(11)	1.806, 1.806
Te(1)–F(2)	1.835(10)	Te(2)–F(7)	1.830(10)	1.821, 1.821
Te(1)–F(3)	1.850(11)	Te(2)–F(8)	1.848(11)	1.805, 1.805
Te(1)–F(4)	1.823(9)	Te(2)–F(9)	1.825(10)	1.808, 1.805
Te(1)–F(5)	1.849(9)	Te(2)–F(10)	1.835(9)	1.819, 1.819

Table 2 (*Continued*)

	Experimental			DFT
Bond angles (°)				
Te(1)–O(1)–Xe(1)	122.3(5)	Te(2)–O(2)–Xe(2)	121.2(6)	124.8, 124.8
O(1)–Te(1)–F(1)	177.7(5)	O(2)–Te(2)–F(6)	178.8(5)	179.2, 179.2
O(1)–Te(1)–F(2)	95.1(5)	O(2)–Te(2)–F(7)	92.6(5)	92.2, 92.2
O(1)–Te(1)–F(3)	91.0(5)	O(2)–Te(2)–F(8)	92.1(5)	89.9, 89.9
O(1)–Te(1)–F(4)	91.2(5)	O(2)–Te(2)–F(9)	90.8(5)	90.7, 90.7
O(1)–Te(1)–F(5)	91.9(5)	O(2)–Te(2)–F(10)	93.5(5)	91.7, 91.7
F(1)–Te(1)–F(2)	87.0(5)	F(6)–Te(2)–F(7)	88.2(5)	88.5, 88.5
F(1)–Te(1)–F(3)	86.8(5)	F(6)–Te(2)–F(8)	87.2(5)	89.4, 89.4
F(1)–Te(1)–F(4)	87.8(5)	F(6)–Te(2)–F(9)	88.2(5)	88.8, 88.8
F(1)–Te(1)–F(5)	89.1(4)	F(6)–Te(2)–F(10)	87.5(5)	88.7, 88.7
F(2)–Te(1)–F(3)	173.8(5)	F(7)–Te(2)–F(8)	175.3(5)	177.8, 177.8
F(2)–Te(1)–F(4)	90.5(5)	F(7)–Te(2)–F(9)	91.4(5)	90.0, 90.0
F(2)–Te(1)–F(5)	88.8(4)	F(7)–Te(2)–F(10)	89.1(5)	89.2, 89.2
F(3)–Te(1)–F(4)	89.9(5)	F(8)–Te(2)–F(9)	88.8(5)	90.3, 90.3
F(3)–Te(1)–F(5)	90.4(4)	F(8)–Te(2)–F(10)	90.3(5)	90.5, 90.5
F(4)–Te(1)–F(5)	176.9(5)	F(9)–Te(2)–F(10)	175.6(4)	177.4, 177.4
O(1)–Xe(1)–O(1A)	180	O(2)–Xe(2)–O(2A)	180	179.5, 179.5
	Experimental	DFT		
$Xe(OSeF_5)_2$				
Bond lengths (Å)				
Xe(1)–O(1)	2.09(3)	2.002, 2.002		
O(1)–Se(1)	1.58(3)	1.698, 1.698		
Se(1)–F(1)	1.70(4)	1.666, 1.666		
Se(1)–F(2)	1.79(2)	1.688, 1.688		
Se(1)–F(3)	1.67(3)	1.667, 1.667		
Se(1)–F(4)	1.81(2)	1.667, 1.667		
Se(1)–F(5)	1.65(3)	1.686, 1.686		
Bond angles (°)				
Se(1)–O(1)–Xe(1)	126(2)	121.8		
O(1)–Se(1)–F(1)	171(2)	179.0		
O(1)–Se(1)–F(2)	91(1)	92.2		
O(1)–Se(1)–F(3)	93(2)	89.8		
O(1)–Se(1)–F(4)	90(1)	90.1		
O(1)–Se(1)–F(5)	96(2)	92.4		
F(1)–Se(1)–F(2)	84(1)	88.4		
F(1)–Se(1)–F(3)	92(1)	89.6		
F(1)–Se(1)–F(4)	82(1)	89.1		
F(1)–Se(1)–F(5)	93(1)	88.5		
F(2)–Se(1)–F(3)	175(1)	177.9		
F(2)–Se(1)–F(4)	82(1)	90.0		
F(2)–Se(1)–F(5)	98(1)	89.4		
F(3)–Se(1)–F(4)	95(1)	90.3		
F(3)–Se(1)–F(5)	85(1)	90.2		
F(4)–Se(1)–F(5)	175(1)	177.5		
O(1)–Xe(1)–O(1A)	180	177.7		

[a] Infrared intensities (km mol^{-1}) are given in parentheses.

temperature structure was affected by a severe three-fold orientational disorder giving rise to unrealistic geometrical parameters. The crystal structure has now been redetermined at −45°C (Fig. 2) and solved in a different space group and with a different three-fold disorder model (see Section 3.4.2). In a previous study, the geometry of $Xe(OTeF_5)_2$ was deduced from a single crystal study using precession camera data, and the study was corroborated by powder data [14]. Although the gross geometry reported agrees with the detailed structure described in this paper (vide infra), the crystallographic parameters differ markedly from those of the present structure (space group *Cmca*, $a = 9.83(5)$ Å, $b = 8.73(5)$ Å, $c = 12.97(5)$ Å, $Z = 4$, $V = 1114$ $Å^3$; cf. Table 1) and suggest that the crystalline material studied was $Xe(OTeF_5)_2$ co-crystallized with another compound.[1]

[1] From the synthetic scheme described in [14], the two most likely components are $FXeOTeF_5$ or $HOTeF_5$. However, based on the difference in volume between the two cells (120 $Å^3$), only one $FXeOTeF_5$ or one $HOTeF_5$ molecule can be accommodated, which is incompatible with the *Cmca* space group. Although it seems unlikely, four XeF_2 molecules would, for example, account for a volume difference of 120 $Å^3$ and would be able to occupy special positions (2/*m*).

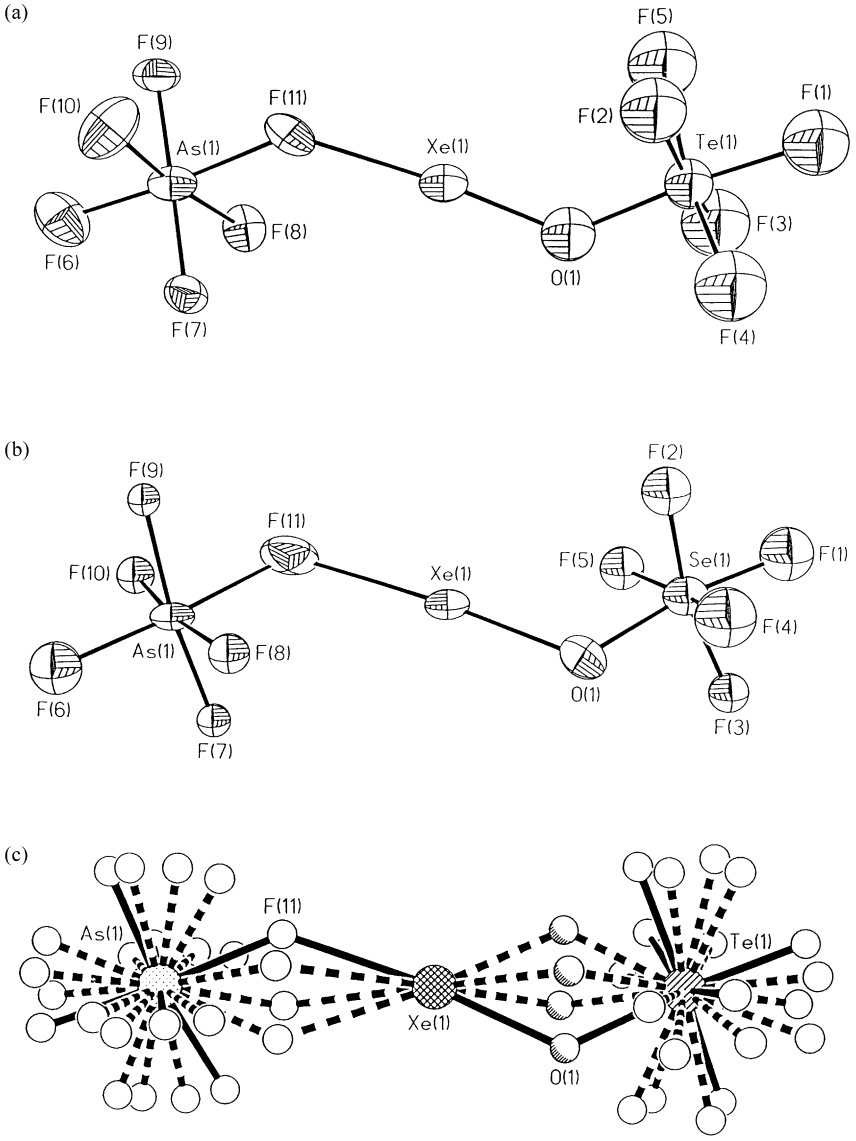

Fig. 1. Structures of (a) $[XeOTeF_5][AsF_6]$ and (b) $[XeOSeF_5][AsF_6]$, thermal ellipsoids are shown at the 50% probability level; (c) disorder model for both $[XeOTeF_5][AsF_6]$ and $[XeOSeF_5][AsF_6]$ (tellurium compound shown).

The crystal structure of $Xe(OTeF_5)_2$ reported in this work is therefore the first reported for this compound.

Three of the four structures reported in the present work suffer orientational disorders of the fluorine and oxygen atoms (four-fold disorders for the $[XeOChF_5][AsF_6]$ salts (Ch = Te, Se) and a three-fold disorder for $Xe(OSeF_5)_2$) which influence the geometrical parameters to some extent. The disorder models are, however, different (see Sections 2.5.1 and 3.4.2). All three compounds crystallized in high symmetry space groups ($P4/n$ or $R\overline{3}$) which require the molecular axes to have only one orientation, allowing the disorder to occur. In contrast, $Xe(OTeF_5)_2$ crystallized in a lower symmetry space group ($P2_1/c$) which requires the molecular axes to have two alternating orientations, favoring an ordered structure (Fig. 3). It is somewhat surprising that, unlike $[XeOTeF_5][AsF_6]$ and $[XeOSeF_5][AsF_6]$, which pack the same way, $Xe(OTeF_5)_2$ and $Xe(OSeF_5)_2$ display different packing arrangements. Although the $Xe(OSeF_5)_2$ structure is disordered, the eclipsed conformation for the equatorial fluorines is preferred and is the same as for the well-resolved $Xe(OTeF_5)_2$ structure. In all four structures, there are fluorine contacts with xenon that are at the limit of the sum of their fluorine and xenon van der Waals radii (3.55 [15]–3.70 [16] Å): 3.321–3.575 Å ($XeOTeF_5^+$), 3.344–3.574 Å ($XeOSeF_5^+$), 3.279–3.634 Å ($Xe(OTeF_5)_2$), 3.370–3.791 Å ($Xe(OSeF_5)_2$).

In the $[XeOChF_5][AsF_6]$ salts, the AsF_6^- anion is fluorine-bridged to the $XeOChF_5^+$ cation through short Xe- - -F contacts ($[XeOTeF_5][AsF_6]$, 2.24(3) Å; $[XeOSeF_5][AsF_6]$, 2.31(4) Å) comparable to that observed in the fluorine analogue, [XeF][AsF_6] (2.212(5) Å) [17], but significantly shorter than that in the isovalent $[F_5TeN(H)Xe][AsF_6]$

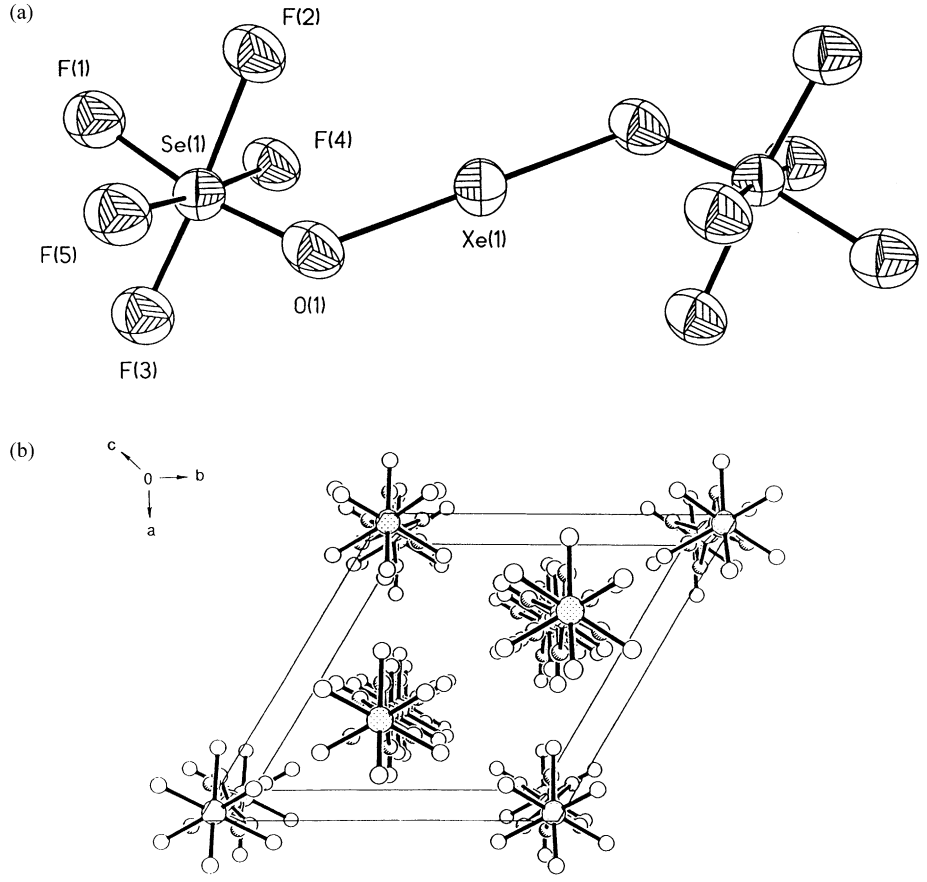

Fig. 2. (a) Structure of $Xe(OSeF_5)_2$, thermal ellipsoids are shown at the 50% probability level. (b) View of the $Xe(OSeF_5)_2$ unit cell along the *c*-axis, for clarity only one orientation is represented.

(2.580(3) Å) salt [18]. It has been previously established for $[XeF][AsF_6]$ [17] and $[XeF][Sb_2F_{11}]$ [19], when compared with XeF_2 [20], that the longer the bridging anion–cation contact, the more covalent the Xe–L bond, L (L = O, F, N). This trend is reflected by the shorter Xe–O bonds in the $[XeOChF_5][AsF_6]$ (Te, 1.96(4) Å; Se, 2.04(4) Å) salts when compared with those in neutral $Xe(OChF_5)_2$ (Te, 2.119(11) and 2.112(12) Å; Se, 2.16(3) Å) and $FXeOSO_2F$ (2.16 Å) [21]. Similar Xe- - -F (2.458(8) Å) and Xe–O (1.962(9) Å) distances have been observed in $HF{\cdot}[HO–TeF_4OXe][AsF_6]$ [22].

The AsF_6^- anions in $[XeOChF_5][AsF_6]$ have distorted octahedral geometries about their arsenic atoms, with bridging As–F bond lengths that are longer ($[XeOTeF_5][AsF_6]$, 1.81(2) Å; $[XeOSeF_5][AsF_6]$, 1.80(4) Å) than the others (average: $[XeOTeF_5][AsF_6]$, 1.72(2) Å; $[XeOSeF_5][AsF_6]$, 1.73(2) Å). The lengthening of the As- - -F_b bond in the AsF_6^- anion, where short anion–cation contacts exist through Xe- - -F_b- - -As fluorine bridges, has also been encountered in $HF{\cdot}[HO–TeF_4OXe][AsF_6]$ (1.771(7) Å versus 1.702(8)–1.722(8) Å) [22], $[XeF][AsF_6]$ (1.813(6) Å versus 1.657(6)–1.690(5) Å) [17], $[F_5TeN(H)Xe][AsF_6]$ (1.740(4) Å versus 1.684(4)–1.712(3) Å) [18] and in $[KrF][AsF_6]$ (1.845(2) Å versus 1.691(2)–1.710(2) Å) [23].

In all structures, the geometries around the chalcogen atoms are pseudo-octahedral with *cis*-F–Ch–F and F–Ch–O angles deviating significantly from 90° in $[XeOTeF_5][AsF_6]$, $[XeOSeF_5][AsF_6]$, and $Xe(OSeF_5)_2$ because of the disorders. The F–Te–F and F–Te–O bond angles in the ordered structure of $Xe(OTeF_5)_2$ are all equal to 90° within experimental error. Although the Se–O (1.58(3) Å) and Se–F (1.65(3)–1.81(2) Å) bond lengths in $Xe(OSeF_5)_2$ are significantly affected by disorder, the Te–O ($[XeOTeF_5][AsF_6]$, 1.85(3) Å; $Xe(OTeF_5)_2$, 1.843(11) and 1.842(11) Å), Te–F ($[XeOTeF_5][AsF_6]$, 1.79(3)–1.84(2) Å; $Xe(OTeF_5)_2$, 1.823(9)–1.855(11) Å), Se–O ($[XeOSeF_5][AsF_6]$, 1.74(4) Å), and Se–F ($[XeOSeF_5][AsF_6]$, 1.70(1) Å) bond lengths in $[XeOChF_5][AsF_6]$ and $Xe(OTeF_5)_2$ are in good agreement with values previously reported for $OSeF_5$ and $OTeF_5$ compounds [24–28].

While the O–Xe–O angles are constrained to be 180° in both the ordered structure of $Xe(OTeF_5)_2$ and the disordered structure of $Xe(OSeF_5)_2$, the O–Xe–F angles only deviate by a few degrees from linearity in the $[XeOChF_5][AsF_6]$ salts (174(1)° (Te) and 174(2)° (Se) and are comparable to that observed previously in $HF{\cdot}[HO–TeF_4OXe][AsF_6]$ (175.6(3)°) [22]. The near linear arrangement of atoms about xenon in these structures is consistent with an AX_2E_3

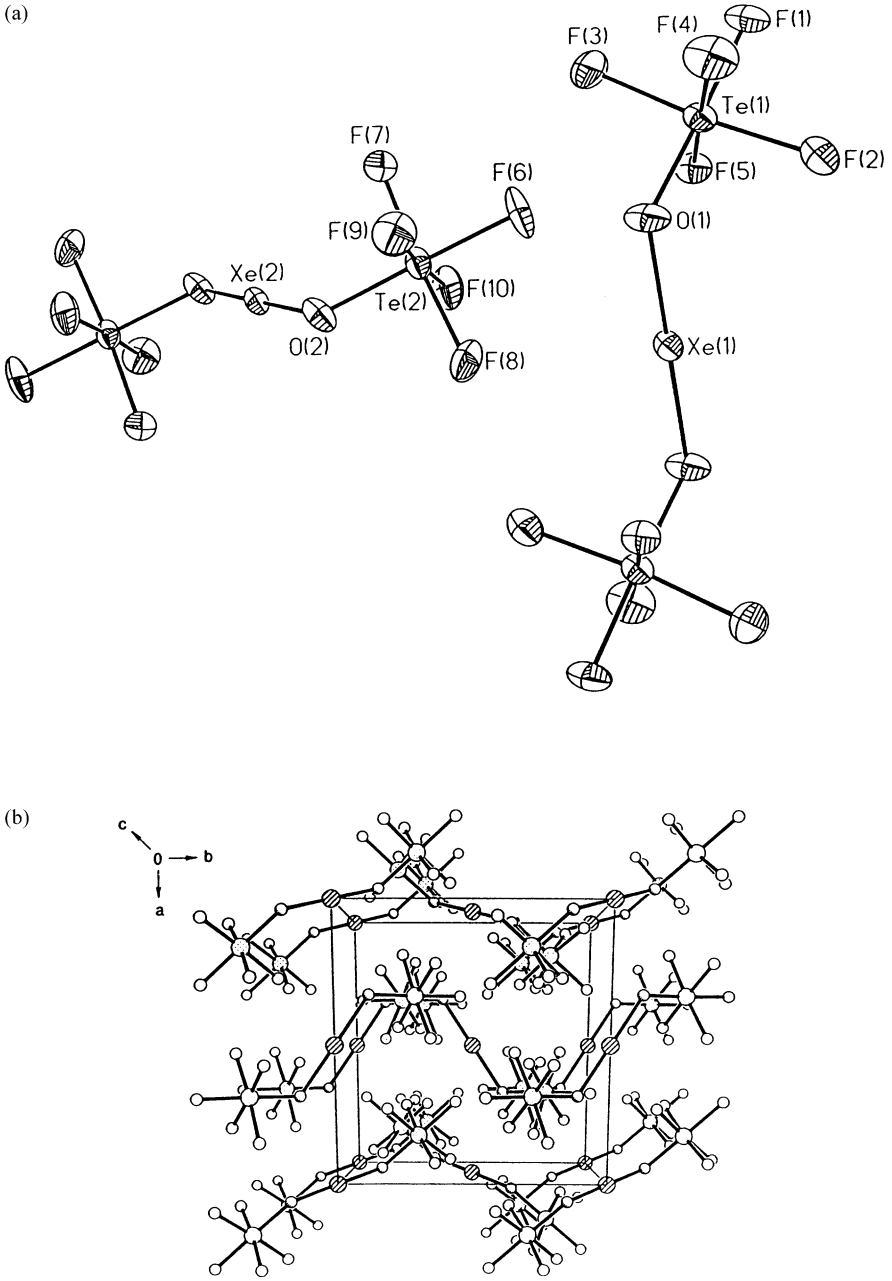

Fig. 3. (a) Structure of $Xe(OTeF_5)_2$, thermal ellipsoids are shown at the 50% probability level. (b) View of the $Xe(OTeF_5)_2$ unit cell along the *c*-axis.

VSEPR arrangement in which the bonding pairs are in axial positions and the lone electron pairs are in equatorial positions [29]. This is supported by the observation that intermolecular secondary contacts around the xenon atom avoid the lone-pair electron density in the equatorial regions of the xenon atoms in the F_5ChO–Xe- - -F–AsF_5 and $Xe(OChF_5)_2$ structures.

The $OChF_5$ groups in $Xe(OChF_5)_2$ and the $OChF_5$ and AsF_6 groups in $[XeOChF_5][AsF_6]$ are arranged *trans* to each other and have Xe–O–Ch and Xe- - -F–As angles that are significantly less than 180° [(As–F–Xe: $[XeOTeF_5][AsF_6]$, 135(1)°; $[XeOSeF_5][AsF_6]$, 129(2)°), (Xe–O–M: $[XeOTeF_5][AsF_6]$, 128(2)°; $[XeOSeF_5][AsF_6]$, 120(3)°; $Xe(OTeF_5)_2$, 122.3(5)° and 121.2(6)°; $Xe(OSeF_5)_2$, 123.9(13)°)]. The bent arrangements about the bridging fluorine and oxygen atoms are in accord with VSEPR AX_2E_2 arrangements [29]. Oxygen bridge angles similar to those observed in the title compounds have also been encountered in $Xe(OTeF_5)_4$ (Xe–O–Te = 125.1(3), 127.7(3)°) [30], $O_2Xe(OTeF_5)_2$ (Xe–O–Te = 130.7(2), 132.5(2)°) [30], $FXeOSO_2F$ (Xe–O–S = 123.7°) [21], and $HF{\cdot}[HO–TeF_4OXe][AsF_6]$ (Xe–O–Te = 123.3(4)°) [22]. Their variability may arise from the deformability of these angles and the space filling requirements of the bulky $OChF_5$ groups.

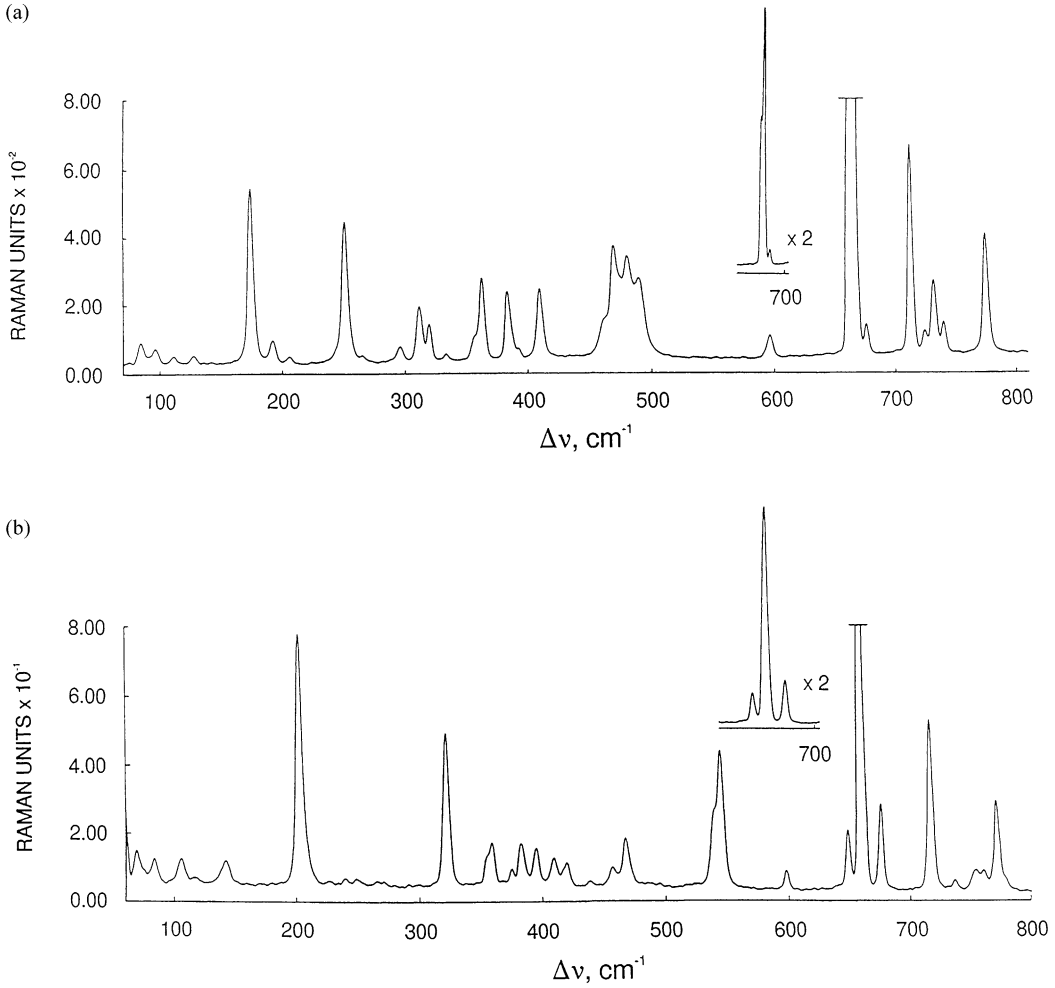

Fig. 4. Raman spectra of microcrystalline (a) $[XeOTeF_5][AsF_6]$ and (b) $[XeOSeF_5][AsF_6]$ recorded in a Pyrex melting point tube at −145°C using 1064-nm excitation.

2.4. Raman spectra of $[XeOChF_5][AsF_6]$ (Ch = Te, Se)

The low-temperature solid-state Raman spectra of $[XeOTeF_5][AsF_6]$ and $[XeOSeF_5][AsF_6]$ are shown in Fig. 4. The observed frequencies and their assignments are summarized in Table 3, along with the calculated frequencies. The Raman spectrum of $[XeOSeF_5][AsF_6]$ is reported for the first time, while that of $[XeOTeF_5][AsF_6]$ [8] has been recorded again and reassigned.

The $XeOChF_5^+$ cations (C_1 point group symmetry) possess 18 fundamental vibrational modes belonging to a single irreducible representation. A factor-group analysis correlating the C_1 point symmetry of the $XeOChF_5^+$ cations to the site symmetry (C_4) and to the crystallographic symmetry (C_{4h}) reveals that each vibrational mode should be split into A_g and E_g Raman-active components, and A_u and E_u infrared-active components under the crystal symmetry.

The fluorine bridged AsF_6^- anions, with distorted octahedral C_s point group symmetry, possess 15 fundamental modes of vibration belonging to the irreducible representations, $10A' + 5A''$. The C_s point group symmetry of the AsF_6^- anion can be correlated to the site symmetry (C_4) and to the crystallographic symmetry (C_{4h}); no bands are predicted to be split in the Raman spectrum.

The spectra of the $XeOChF_5^+$ cations were assigned by comparison with the frequencies obtained from DFT calculations and with those obtained previously for $[XeOTeF_5][Sb_2F_{11}]$ [8]. The modes of the distorted AsF_6^- anion were assigned by comparison with those calculated recently for the $[KrF][AsF_6]$ ion pair [23,31] and those observed for other AsF_6^- salts [32,33]. The spectra of $Xe(OChF_5)_2$ have also been assigned in Table 4 by comparison with the frequencies obtained from DFT calculations and are supported by Raman polarization measurements made previously on $Xe(OSeF_5)_2$ for which infrared data are also available [34].

2.5. Computational results

In order to improve the vibrational assignments and gain more information about the structures and bonding in $XeOChF_5^+$ and $Xe(OChF_5)_2$ (Ch = Se, Te), electron

Table 3
Experimental Raman frequencies for $[XeOTeF_5][Sb_2F_{11}]$, $[XeOChF_5][AsF_6]$ and calculated vibrational frequencies, assignments, and mode descriptions for $XeOChF_5^+$ (Ch = Se, Te)

Frequencies (cm^{-1})			Assignments		Frequencies (cm^{-1})		Assignments	
$[XeOTeF_5][Sb_2F_{11}]$[a,b]	$[XeOTeF_5][AsF_6]$[b]	$XeOTeF_5^+$ (DFT)[c]	$XeOTeF_5^+$ (C_1)[d]	AsF_6^- (C_s)[e]	$[XeOSeF_5][AsF_6]$[a,b]	$XeOSeF_5^+$ (DFT)[c]	$XeOSeF_5^+$ (C_1)[d]	AsF_6^- (C_s)[e]
	775(24)			A″	760(4)			A″
					754(4)			
	724(4)			A′	736(2)			A′
					730(<1)			
	701(1)			A′				
748(2)		739(78)	ν_{as}(TeF1 − TeO) + ν_{as}(TeF5 − TeF4) + ν_{as}(TeF2 − TeF3)		779(3), sh	778(119)	ν_{as}(SeF5 − SeF4) + ν_{as}(SeF2 − SeF3) + some ν(SeF1)	
741(14)	739(6)	734(89)	ν_{as}(TeF2 − TeF3)		771(21)	775(128)	ν(SeF1)	
	731(13)	728(76)	ν_{as}(TeF5 − TeF4)			772(135)	ν_{as}(SeF5 − SeF4) + ν_{as}(SeF2 − SeF3)	
714(23)	712(41)	680(35)	ν_{as}(TeO − XeO) + some ν_s(TeF5)		717(39)	685(19)	ν_s(SeF5 + SeF2) + ν_s(SeF3 + SeF4) + ν_{as}(SeO − XeO)	
	676(6)			A′	676(20)			A′
671(64)	667(100)	651(6)	ν_s(TeF2 + TeF3)		659(100)	643(13)	ν(XeO) − ν(SeO)	
661(31)	662(58), sh	643(3)	ν_s(TeF5 + TeF4)		649(14)	641(4)	ν_s(SeF5 + SeF4) − ν_s(SeF2 + SeF3)	
	596(<1)			A′	598(4)			A′
487(41)	491(14)	485(25)	ν_s(TeO + XeO)		545(32)	517(30)	ν(XeO) + ν(SeO)	
	481(17)				539(16), sh			
474, sh	470(19)				468(10)	440(130)	δ(F5F2F3F4) umbrella	
	462(7), sh				458(5)	435(33)	δ(F2F3F1) o.o.p.	
						432(23)	δ(F4F5F1) o.o.p. + δ(F2SeO)	
					438(2)	419(3)	δ(F5SeF2) + δ(F3SeF4)	
					420(5)			[f]
	409(12)			[f]	409(6)			[f]
	392(2)			[f]	395(8)			[f]
	383(12)			A″	382(9)			A″
					374(3)			A′
					358(9)	364(4)	F1SeO rock − (F5SeF4 rock + F2SeF3 rock)	
	362(14)			A″				
	355(4), sh			A′	355(6), sh			A′
		339(66)	δ(F5TeF3) + some δ(F1TeF3)					
		334(35)	δ(F5TeF2) + some δ(F3TeF4)					
	333(1)	331(28)	δ(F3TeF4) + some δ(F1TeF3)					
320(4)	320(6)	322(29)	δ(F2F3F1) o.o.p.		322(35)	340(2)	δ(F1SeO) + δ(F5SeF2) − δ(F3SeF4)	
311(10)	311(9)							
293(9)	295(3)	292(3)	δ(F2TeO) − δ(F3TeF1)					
					271(1)			A′
	264(1)			A″	265(1)			A″
252(28)	251(28)	261(0)	δ(F5TeF1) − δ(F4TeO) + some δ(F2TeF3)					
					248(2)	274(0)	δ(F2SeO) − δ(F3SeF1) + δ(F5SeF4)	
					240(2)			
	223(<1)			A′	226(1)			A′

Table 3 (*Continued*)

Frequencies (cm^{-1})			Assignments		Frequencies (cm^{-1})		Assignments	
$[XeOTeF_5][Sb_2F_{11}]$[a,b]	$[XeOTeF_5][AsF_6]$[b]	$XeOTeF_5^+$ (DFT)[c]	$XeOTeF_5^+$ (C_1)[d]	AsF_6^- (C_s)[e]	$[XeOSeF_5][AsF_6]$[a,b]	$XeOSeF_5^+$ (DFT)[c]	$XeOSeF_5^+$ (C_1)[d]	AsF_6^- (C_s)[e]
210(3)	205(1)	216(0)	δ(F5TeF4) − δ(F2TeF3) (towards O)		203(58)	227(0)	δ(F1SeO) i.p. bisecting ∠ F4SeF2	
	192(4)	183(0)	δ(F1TeO) in F2F1F3TeO plane		196(1)	205(0)	δ(F1SeO) i.p. bisecting ∠ F5SeF2	
173(31)	174(34)	169(1)	δ(F1TeO) in F5F1F4TeO plane					
					142(5)			A′
125(4)	127(1)	103(2)	δ(XeOTe) approximately in XeOF1Te plane					
					106(5)	112(1)	δ(XeOSe) approximately in XeOF1Se plane	
		56(1)	Te–O torsion			61(1)	Se–O torsion	
	111(1)		Lattice modes		117(2)		Lattice modes	
	96(3)				95(<1)			
	84(4)				83(5)			
	75(<1)				75(3), sh			
					69(7)			

[a] Values taken from [8].
[b] Spectra recorded on microcrystalline powders in Pyrex glass capillaries at −145°C using 1064-nm excitation. Values in parentheses denote relative Raman intensities; sh, shoulder.
[c] Infrared intensities (km mol^{-1}) are given in parentheses.
[d] The atom numbering scheme is given in Fig. 1; o.o.p. and i.p. denote out-of-plane and in-plane bends, respectively.
[e] The AsF_6^- anion is assigned under C_s point symmetry as described in [23].
[f] Similar bands have been observed in other AsF_6^- salts but are not assigned.

Table 4
Experimental Raman and calculated vibrational frequencies, assignments, and mode descriptions for $Xe(OChF_5)_2$ (Ch = Se, Te)

$Xe(OTeF_5)_2$			$Xe(OSeF_5)_2$			
Frequencies (cm^{-1})		Assignments	Frequencies (cm^{-1})			Assignments
Experimental[a]	DFT[b]	C_2[c]	Experimental[d]		DFT[b]	C_2[c]
796(3)	790(0)	ν_s(TeO + Te′O′) + ν(XeO_2)	791(2)	[788, m]	795(7)	ν_s(SeO + Se′O′) + ν(XeO_2)
788(5)						
785(2)						
730(4)	750(903)	ν_{as}(TeO − Te′O′) + ν(XeO_2)		[725, vs]	755(701)	ν_{as}(SeO − Se′O′) + ν(XeO_2)
710, sh	706(205)	ν_{as}(TeF4 − TeF5) + ν_{as}(Te′F4′ − Te′F5′)	731(4)		740(194)	ν_{as}(SeF4 − SeF5) + ν_{as}(Se′F4′ − Se′F5′)
708, sh	706(242)	ν_{as}(TeF2 − TeF3) + ν_{as}(Te′F2′ − Te′F3′) + ν_{as}(TeF4 − TeF5) + ν_{as}(Te′F4′ − Te′F5′)		[699, s]	738(404)	ν_{as}(SeF4 − SeF5) − ν_{as}(Se′F4′ − Se′F5′)
706(7)	705(31)	ν_{as}(TeF2 − TeF3) + ν_{as}(Te′F2′ − Te′F3′)			737(148)	ν_{as}(SeF2 − SeF3) + ν_{as}(Se′F2′ − Se′F3′)
701(9)	704(8)	ν_{as}(TeF2 − TeF3) − ν_{as}(Te′F2′ − Te′F3′) + ν_{as}(TeF4 − TeF5) − ν_{as}(Te′F4′ − Te′F5′)			735(175)	ν_{as}(SeF2 − SeF3) − ν_{as}(Se′F2′ − Se′F3′)
690(27)	683(99)	ν_{as}(TeF1 − Te′F1′)	690(9)		713(156)	ν_{as}(SeF1 − Se′F1′)
	679(0)	ν_s(TeF1 + Te′F1′)			704(7)	ν_s(SeF1 + Se′F1′) − ν_s(XeO + XeO′) + some ν_s(SeO + Se′O′)
647(22)	629(0)	$\nu_s(TeF_4)_{eq}$ − ν(TeF1) + $\nu_s(Te'F_4')_{eq}$ − ν(Te′F1′)	631(28)	[638, w]	630(0)	$[\nu_s(SeF_4)_{eq} - \nu_s(SeF1)] + [\nu_s(Se'F_4')_{eq} - \nu_s(Se'F1')]$
639(10)	623(49)	ν_s(Te′F4′ + Te′F5′) − ν_s(TeF4 + TeF5)		[612, s]	626(78)	$\nu_s(SeF_4)_{eq} - \nu_s(Se'F_4')_{eq} + \nu_{as}$(OXeO′)
635(14)	622(3)	ν_s(TeF4 + TeF5) − ν_s(TeF2 + TeF3) + ν_s ($Te'F_4'$ + Te′F5′) − ν_{as}(Te′F2′ + Te′F3′)			610(5)	ν_{as}(Se′F2′ + Se′F3′) − ν_s(Se′F4′ + Se′F5′) + ν_s(SeF4 + SeF5) − ν_s(SeF2 + SeF3)
	621(6)	ν_s(TeF2 + TeF3) − ν_s(Te′F2′ + Te′F3′)			610(5)	ν_s(SeF4 + SeF5) − ν_s(SeF2 + SeF3) + ν_s(Se′F2′ + Se′F3′) − ν_s(Se′F4′ + Se′F5′)
	547(77)	ν_s(XeO + TeO) − ν_s(XeO′ + Te′O′) + δ(OXeO′)			611(21)	ν_s(XeO + XeO′) + ν_s(SeO + Se′O′) + δ(OXeO′)
440(100)	474(0)	ν_s(XeO + TeO) + ν_s(XeO′ + Te′O′) + δ(XeOTe) + δ(XeO′Te′)			552(3)	ν_s(OXeO′)
445, sh						
428(27)						
	360(1)	$\delta_s[(TeF_4)_{eq}$ umbrella + $(Te'F_4')_{eq}$ umbrella]			469(3)	$\delta_s[(SeF_4)_{eq}$ umbrella + $(Se'F_4')_{eq}$ umbrella]
	355(241)	$\delta_{as}[(TeF_4)_{eq}$ umbrella − $(Te'F_4')_{eq}$ umbrella]	433(3)	[431, s]	460(319)	$\delta_{as}[(SeF_4)_{eq}$ umbrella − $(Se'F_4')_{eq}$ umbrella]
	345(84)	F5F4F1O umbrella + F2′F3′F1′O′ umbrella	421(2)	[423, m]	450(77)	δ(OXeO′) o.o.p. + ($OSeF_5$) bends
	344(14)	F5F4F1O umbrella − F2′F3′F1′O′ umbrella			449(4)	
	340(5)	($OTeF_5$) bends	394(1)		440(4)	SeF_5 bends
332(2)	337(34)	TeF_5 bends			440(48)	
328(2)	332(1)	TeF_5 bends + δ(OXeO′) o.o.p.	380(2)		412(3)	δ(OXeO′) o.o.p. + ($OSeF_5$) bends
320(4)	320(1)	TeF_5 bends + torsion of OXeO′ around Xe			407(2)	($OSeF_5$) bends + torsion of OxeO′ around Xe
304(5)	304(0)				401(0)	
297, sh	304(0)				400(0)	SeF_5 bends
	266(40)		300(38)	[305, w]	338(31)	
247(13)	254(0)	TeF_5 bends			329(0)	($OSeF_5$) bends
240(30)						
234(13)	234(0)		248(1)		297(0)	($OSeF_5$) bends
	229(4)				293(0)	SeF_5 bends
212(1)	212(0)	TeF_5 bends + δ(OXeO′) o.o.p.			271(0)	δ(OXeO′) o.o.p. + ($OSeF_5$) bends

Table 4 (*Continued*)

$Xe(OTeF_5)_2$			$Xe(OSeF_5)_2$		
Frequencies (cm^{-1})		Assignments	Frequencies (cm^{-1})		Assignments
Experimental[a]	DFT[b]	C_2[c]	Experimental[d]	DFT[b]	C_2[c]
203(1)	206(17)	($OTeF_5$) bends + torsion of OXeO′ around Xe		265(0)	($OSeF_5$) bends + torsion of OXeO′ around Xe
192(2)	199(12)	($OTeF_5$) bends + torsion of OXeO′ around Xe	196(1)	240(48)	ν_{as}(OXeO′), Xe moving
188(2)					
	147(0)	TeF_5 rock about O i.p.	158(100)	179(0)	($OSeF_5$) bends
	145(0)	TeF_5 rock about O i.p.		170(1)	δ(OXeO′) i.p.
133(39)	137(0)	δ(OXeO′), Xe moving o.o.p. + TeF_5 rock about O	132(40)	159(1)	δ(OXeO′) o.o.p.
130(37)					
123(7)					
120(6)					
115(2)					
66(10)	70(0)	δ(XeOTe) + δ(XeO′Te′)	77(8)	95(0)	$XeO(SeF_5)$ bend o.o.p.
48(9)	62(0)	$XeO(TeF_5)$ bend o.o.p. asymmetry		94(0)	δ(XeOSe) + δ(XeO′Se′)
39(11)	55(0)	$XeO(TeF_5)$ bend o.o.p. symmetry		80(0)	Torsion of SeF_5 about SeO
32(11)	53(0)	δ(XeOTe) − δ(XeO′Te′)		71(1)	δ(XeOSe) − δ(XeO′Se′)
	41(0)	Torsion of TeF_5 about TeO		64(0)	$XeO(SeF_5)$ bend o.o.p.

[a] Raman frequencies are taken from [8].

[b] Infrared intensities (km mol^{-1}) are given in parentheses.

[c] Atoms designated with 'prime' denote the symmetry equivalents of atoms labeled F1, F2, F3, F4, F5, F6, and O in Figs. 2 and 3. The abbreviations o.o.p. and i.p. denote out-of-plane and in-plane bends, respectively.

[d] Raman and infrared (values in square brackets) frequencies are taken from [34].

structure calculations at the DFT level were carried out on both gas phase species, as well as on the ion pair derived from AsF_6^- and $XeOChF_5^+$. We have shown that this level of calculation gives good results for this series of compounds and for several F_5TeN-derivatives [18]. We also calculated the geometries and vibrational frequencies for TeF_6 and SeF_6 as benchmarks. The calculated M–F bond distances for MF_6 are 1.801 Å (Te) and 1.662 Å (Se), compared with the experimental values of 1.815(2) Å (Te) [35] and 1.688(10) Å (Se) [36]. The TeF (SeF) stretches are calculated to be at 721 (761) (T_{1u}), 659 (693) (A_{1g}) and 637 (631) (E_g) cm^{-1}, compared with the experimental values at 751 (780) (T_{1u}), 697 (708) (A_{1g}) and 670 (658) (E) cm^{-1} [37,38]. The bends are calculated to be at 314 (455) (T_{1u}), 298 (412) (T_{2g}) and 183 (281) (T_{2u}) cm^{-1}, compared with the experimental values at 325 (437) (T_{1u}), 312 (403) (T_{2g}) and 197 (264) (T_{2u}) cm^{-1} [37,38]. The calculated values are in good agreement with experiment, with the DFT values about 30–40 cm^{-1} too low for the Ch–F stretches and 10–20 cm^{-1} too low (Te) and too high (Se) for the bends.

2.5.1. Geometries

2.5.1.1. $XeOChF_5^+$. The calculated ChF_5 geometries are in good agreement with the experimental ones (Table 2). The two Ch–F_e bonds that are closest to the XeO group are slightly longer than the other two Ch–F_e bonds. The calculated Ch–F_a bond is shorter than the Ch–F_e bonds by about 0.01 (Te) and 0.02 (Se) Å. The calculated Ch–O bond lengths are too long by 0.12 (Te) and 0.11 (Se) Å, whereas the calculated Xe–O bond lengths are too short by 0.07 (Te) and 0.14 (Se) Å. This discrepancy arises from the strong interaction of Xe with the AsF_6^- anion, which leads to a weaker Xe–O interaction than in the isolated cation. This is consistent with Hartree–Fock (HF) calculations done on the $[XeOTeF_5][AsF_6]$ ion pair. In this case, although the Xe–F_b bond distance of 2.01 Å is far too short when compared with the experimental value of 2.24 Å, the Te–O bond length shortens to 1.850 Å and the Xe–O bond length lengthens to 1.966 Å, in agreement with experiment. Two conformers having C_1 point symmetry are found for the energy minimized gas phase structures of the $XeOChF_5^+$ cations (Table 2). The Xe–O–Ch plane is rotated so that it is staggered, but does not quite lie in the plane that bisects the angle subtended by two equatorial fluorine atoms of the ChF_5 group, i.e., the equatorial TeF_4 group is rotated by 34.1° (Te) and 44.5° (Se) relative to the [F_aTeOXe] plane. In contrast, this angle is 36° (Te) and 48° (Se) in the experimental structures; the deviations from the calculated values are most likely related to disorder and/or crystal packing.

2.5.1.2. $Xe(OChF_5)_2$. The calculated geometry for $Xe(OTeF_5)_2$ is in good agreement with the experimental one, except for the calculated Xe–O bond length which is too short by 0.12 Å (Table 2) as found in $XeOTeF_5^+$. The Te–F and Te–O bond lengths are in good agreement with the experimental values as we would expect from the results for the $XeOTeF_5^+$ cation. The calculated Te–O bond length is only 0.01–0.02 Å longer than the Te–F bond lengths. The calculated geometry for $Xe(OSeF_5)_2$ differs from that observed experimentally, but we note that a 'multi-site' positional disorder induced errors in the geometrical parameters (see Section 3.4.2). The calculated Xe–O bond length is again too short, this time by 0.09 Å. The calculated Se–F bond lengths are all about 1.67 Å and that of Se–O is 1.70 Å. The calculated Se–O bond length is only 0.01–0.02 Å longer than the Se–F bond lengths. Considering the good agreement between the calculated and experimental geometries for $XeOSeF_5^+$, it is likely that the calculated geometry is more reliable except for the Xe–O bond length. The calculated Xe–O bond length is slightly longer in $Xe(OSeF_5)_2$ than in the tellurium analogue, consistent with the higher electronegativity of the $OSeF_5$ group. Two conformers having C_2 point symmetry are found for the energy minimized gas-phase structures of $Xe(OChF_5)_2$ (Table 2). For $Xe(OTeF_5)_2$, the F_a, Te, O, and Xe atoms lie in the same plane, as observed experimentally. The two equatorial TeF_4 groups are rotated by ~45° relative to the [F_a, Te, O, Xe] plane and are not quite eclipsed. This differs from experiment, where this angle is 32° and the eclipsed conformation of the two equatorial TeF_4 groups is imposed by symmetry. For $Xe(OSeF_5)_2$, the torsion angle between the O–Se–Xe and O′–Se′–Xe planes is ~26°, and each equatorial SeF_4 group is rotated by ~45° from their respective Se–O–Xe plane. Experimentally, the F_a, Se, O and Xe atoms are found to be coplanar, but the staggered conformation is also observed for the equatorial SeF_4 groups, with an angle of 43° (Se); the two equatorial SeF_4 groups are almost eclipsed. Again, the deviations from the calculated values are most likely related to disorder and/or crystal packing.

2.5.2. Vibrational frequencies

The calculated vibrational frequencies for $XeOChF_5^+$ and $Xe(OChF_5)_2$ are compared with the experimental values in Tables 3 and 4. In general, the trends observed for the stretching frequencies associated with the ChF_5-group follow those given for ChF_6 and, as expected, the Te–O and Te–F frequencies are found to be lower than the Se–O and Se–F ones. The calculated Te–F stretches in $XeOTeF_5^+$ are slightly greater than or equal to the values in TeF_6 with three Te–F stretches (739, 734, 728 cm^{-1}) derived from the T_{1u} band, and the other two TeF stretches (651, 643 cm^{-1}) derived from the E_g mode. The Te–F stretching frequencies are all similar to what is found in F_5TeN-derivatives that we have calculated [18]. A number of the previous assignments for $XeOTeF_5^+$ [8] have been reassigned based on the calculated spectrum. For example, the frequency corresponding to the asymmetric combination of the Xe–O and Te–O stretches is at 680 cm^{-1}, much higher than the previous assignment at 470, 476 cm^{-1} and slightly above a

number of the Te–F stretching frequencies. It is worth noting that calculations on the ion pair show that there is a coupling of the stretches involving O with the As–F modes near 750 cm^{-1} as well as some coupling to a mode near 550 cm^{-1}. The predicted Te–O + Xe–O symmetric stretch at 485 cm^{-1} is consistent with the previously assigned values of 483, 492 cm^{-1}. These stretches are above the strongly coupled Te–N and Xe–N stretches in the $F_5TeN(H)Xe^+$ cation, 623 cm^{-1} (ν(Xe–N − Te–N)) and 432 cm^{-1} (ν(Xe–N − Te–N)) [18]. The XeOTe bend is also found to be lower at 103 cm^{-1} compared with 174 cm^{-1} in the previous assignment. Similar modes had also been incorrectly assigned in $Xe(OTeF_5)_2$ [8]. In the infrared and Raman spectra of $Xe(OSeF_5)_2$ [34], we find that the assignment for the mode observed at 725 cm^{-1} should be changed to an SeO asymmetric stretch since it is expected to be the most intense mode in the infrared spectrum.

2.5.3. Mayer bond orders and valencies, and Mulliken charges

The Mulliken charges, Mayer valencies and Mayer bond orders [39–42] are given in Table 5. The valencies for Te are near 6.3 and those for Se are near 6.2 as expected for the hexacoordination. The valencies of the F atoms are all more than 1 ranging from 1.1 to 1.2. The oxygen atoms have valencies of approximately 2 as expected for two-coordinate oxygen atoms. The xenon atoms have valencies of 1.8 in the $Xe(OChF_5)_2$ and this value is reduced to ∼1.25 in the $XeOChF_5^+$ cations. The Ch–F bond orders range from 0.99 to 1.15 for the various compounds, showing essentially single Ch–F bonds. The Ch–O bond orders differ significantly in $Xe(OChF_5)_2$ when compared with the $XeOChF_5^+$ cations, with bond orders in the bis-compounds being about 1.1 and those in the cations being about 0.8, a clear difference. This is consistent with significant lengthening of the Ch–O bond in going from the bis-compounds to the cations. The Xe–O bond orders show the opposite behavior with the bond order in $Xe(OChF_5)_2$ being 0.82 and the bond order in the cation being 1.12. Again, there is a correlation as the Xe–O bond distances decrease from 2.00 Å in $Xe(OChF_5)_2$ to 1.90 Å in $XeOChF_5^+$.

A natural bond orbital (NBO) analysis [43,44] was also performed with a polarized double-ζ basis set [39–43,46] at the DFT level (Table 6). The natural population analysis (NPA) given in Table 7 predicts the chalcogen and xenon to have more positive charge and the F and O to have more negative charge than does the Mulliken analysis. The NPA gives charges of 3.45 and 3.45 (Te) and 2.78 and 2.94 (Se) for $XeOChF_5^+$ and $Xe(OChF_5)_2$, respectively. The Xe has a charge of 1.1–1.2e for both the cations and the bis-compounds. The NPA shows a larger degree of charge separation (corresponding to more ionic bond character) than does the Mulliken charge analysis, but both are consistent with significantly ionic structures. The NBO analysis shows that the Ch–F bonds are highly ionic with 80–90% of the nominal two electrons in the bond being on the F. The electrons on the F are found to be in orbitals having high p character. The chalcogen in the Ch–F bonds has a low valence s population and higher p and d populations. The Ch–O bonds are similar to the Ch–F bonds in terms of their make-up. There are about 0.2e in the σ^* orbitals for the Ch–F and Ch–O bonds. The Xe–O bonds in the cations show that there is about 40% of the bond on the Xe and 60% on the O. The bond is essentially pure valence p in character on both the O and the Xe. We were unable to find two Xe–O bonds in the $Xe(OChF_5)_2$ compounds as the NBO analysis only yielded one Xe–O bond even though there are two symmetric Xe–O interactions. The latter finding is consistent with the valence bond

Table 5
Atomic charges, Mayer valencies and Mayer bond orders for $XeOChF_5^+$, and $Xe(OChF_5)_2$ (Ch = Se, Te)

Atom	$XeOTeF_5^+$	$XeOSeF_5^+$	$Xe(OTeF_5)_2$	$Xe(OSeF_5)_2$
Atomic charges and Mayer valencies[a]				
Ch(1)	1.32 [6.31]	1.06 [6.24]	1.31 [6.34]	1.05 [6.24]
F(1)	−0.18 [1.22]	−0.12 [1.24]	−0.25 [1.10]	−0.19 [1.12]
F(2)	−0.22 [1.14]	−0.17 [1.14]	−0.27 [1.07]	−0.22 [1.07]
F(3)	−0.18 [1.20]	−0.12 [1.23]	−0.25 [1.11]	−0.20 [1.12]
F(4)	−0.18 [1.22]	−0.12 [1.23]	−0.25 [1.10]	−0.20 [1.12]
F(5)	−0.22 [1.12]	−0.17 [1.14]	−0.26 [1.07]	−0.22 [1.08]
O(1)	−0.16 [1.98]	−0.17 [1.96]	−0.30 [2.07]	−0.29 [2.01]
Xe(1)	0.82 [1.24]	0.82 [1.25]	0.50 [1.78]	0.53 [1.80]
Mayer bond orders				
Ch(1)–F(1)	1.14	1.16	1.04	1.05
Ch(1)–F(2)	1.06	1.04	1.00	0.99
Ch(1)–F(3)	1.11	1.11	1.05	1.05
Ch(1)–F(4)	1.11	1.11	1.05	1.05
Ch(1)–F(5)	1.03	1.04	1.01	1.00
Ch(1)–O(1)	0.81	0.75	1.13	1.05
Xe(1)–O(1)	1.12	1.12	0.81	0.82

[a] Mayer valencies are reported in square brackets.

Table 6
Natural bond order analysis for the $XeOChF_5^+$ cations and $Xe(OChF_5)_2$ (Ch = Se, Te)

Orbital	Orbital population		%s	%p	%d
$XeOTeF_5^+$					
σ(Te–F)	1.88–1.89	[Te (13–15%)] [F (85–87%)]	15–18	50–55 84–86	27–34
σ(Te–O)	1.88	[Te (12%)] [O (88%)]	14	46 83	40
σ(Xe–O)	1.99	[Xe (39%)] [O (61%)]	7	92 91	1
σ*(Te–F)	0.17–0.18				
σ*(Te–O)	0.20				
σ*(Xe–O)	0.04				
$XeOSeF_5^+$					
σ(Se–F)	1.85–1.86	[Se (18–20%)] [F (80–82%)]	16–18	50–54 90	28–34
σ(Se–O)	1.88	[Se (17%)] [O (83%)]	15	47 90	39
σ(Xe–O)	1.99	[Xe (43%)] [O (57%)]	5	95 94	0
σ*(Se–F)	0.21–0.22				
σ*(Se–O)	0.24				
σ*(Se–O)	0.07				
$Xe(OTeF_5)_2$					
σ(Te–F)	1.88–1.89	[Te (12–13%)] [F (87–88%)]	16–17	49–52 83	32–35
σ(Te–O)	1.88	[Te (16%)] [O (84%)]	19	49 78	32
σ*(Te–F)	0.18–0.19				
σ*(Te–O)	0.18				
$Xe(OSeF_5)_2$					
σ(Se–F)	1.86–1.88	[Se (16–17%)] [F (83–84%)]	16–17	49–51 85	32–35
σ(Se–O)	1.88	[Se (22%)] [O (78%)]	19	49 79–81	31
σ*(Se–F)	0.20–0.21				
σ*(Se–O)	0.19				

descriptions I and II of XeL_2 and XeL (L = $OChF_5$), where structures $[L^-Xe^{2+}L^-]$ and $[Xe^{2+}L^-]$ are the least important contributing structures. Accordingly, the $Xe(OChF_5)_2$ molecules have formal Xe–O bond orders of $\frac{1}{2}$ and the formal Xe–O bond order for the $XeOChF_5^+$ cations is 1, in qualitative agreement with the Mayer bond orders and NBO analyses.

$$L^-Xe^{2+}L^- \leftrightarrow L{-}Xe^+L^- \leftrightarrow L^-Xe^+{-}L \quad (I)$$

$$Xe{-}L^+ \leftrightarrow Xe^{2+}L^- \quad (II)$$

Table 7
NPA for the $XeOChF_5^+$ cations and $Xe(OChF_5)_2$ (Ch = Se, Te)

Atom	$XeOTeF_5^+$	$XeOSeF_5^+$	$Xe(OTeF_5)_2$	$Xe(OSeF_5)_2$
Ch	3.45	2.78	3.45	2.94
F5	−0.58	−0.47	−0.58	−0.50
F2	−0.57	−0.47	−0.60	−0.53
F3	−0.54	−0.41	−0.58	−0.50
F1	−0.54	−0.42	−0.58	−0.50
F4	−0.53	−0.42	−0.60	−0.53
O	−0.88	−0.70	−1.10	−0.97
Xe	1.18	1.11	1.17	1.16

3. Experimental

3.1. Apparatus and materials

Manipulations involving volatile materials were performed under anhydrous conditions as previously described [46]. The syntheses of XeF_2 [47], $[XeOTeF_5][AsF_6]$ [7], $Xe(OTeF_5)_2$ [6], $Xe(OSeF_5)_2$ [6] and AsF_5 [47] have been described elsewhere; and SbF_5 (Ozark Mahoning) [48] and BrF_5 (Matheson) [49] were purified as previously described.

Freon-114 (Aldrich) was dried over P_4O_{10} and vacuum distilled into a dry Pyrex storage vessel prior to use.

3.1.1. $FXeOSeF_5$

Stoichiometric amounts of $Xe(OSeF_5)_2$ (1.7524 g, 3.438 mmol) and XeF_2 (0.5816 g, 3.436 mmol) were loaded into a 9 mm NMR tube in a drybox at room temperature, closed with a Kel-F valve and warmed to 45°C, whereupon the sample melted, yielding a pale yellow liquid and with solid XeF_2 remaining at the bottom of the sample. After ca. 15 min, all XeF_2 had dissolved and upon standing; the liquid $FXeOSeF_5$ became colorless (2.362 g, 6.941 mmol).

3.1.2. $[XeOSeF_5][AsF_6]$

The salt, $[XeOSeF_5][AsF_6]$, was prepared by addition of a stoichiometric excess of AsF_5 to liquid $FXeOSeF_5$ (2.3615 g, 6.941 mmol) in a 9 mm FEP reactor at room temperature. The sample was agitated as gaseous AsF_5 was slowly bled into the reactor through a Kel-F valve whereupon a light yellow solid formed. The AsF_5 pressure was increased to 1 atm and the solid sample powdered. After several hours, the AsF_5 pressure was increased to 2 atm and maintained at this pressure for 12 h followed by removal of excess AsF_5 under vacuum. The sample was pumped under dynamic vacuum for several minutes at room temperature, yielding 3.453 g (6.769 mmol) of $[XeOSeF_5][AsF_6]$ (theor. 3.498 g).

3.2. NMR sample preparation

Samples of $[XeOSeF_5][AsF_6]$ for ^{19}F, ^{77}Se, and ^{129}Xe NMR spectroscopy (see Section 3.5) were prepared in 4 and 9 mm FEP tubes, respectively, fitted with Kel-F valves. After the solute and solvent had been added, the sample tubes were heat sealed and inserted into 5 and 10 mm thin-walled precision glass NMR tubes (Wilmad), respectively, as previously described [50]. A ^{19}F sample employing BrF_5 as the solvent was prepared by condensing BrF_5 onto $[XeOSeF_5][AsF_6]$ at −196°C followed by warming to −40°C to effect dissolution. Fluorine-19, ^{77}Se and ^{129}Xe samples employing SbF_5 as the solvent were prepared by adding SbF_5 to FEP sample tubes using a glass syringe inside a dry nitrogen-filled glove bag. The SbF_5 samples were transferred to a drybox equipped with a cryowell, where the SbF_5 was frozen and $[XeOSeF_5][AsF_6]$ was added. The samples were warmed to room temperature on a metal vacuum line under 1 atm of dry nitrogen whereupon slow evolution of AsF_5 occurred. The AsF_5 pressure was periodically reduced by pumping the N_2/AsF_5 mixture down to 1 atm. When AsF_5 evolution ceased, the samples were cooled to −78°C and evacuated to remove residual AsF_5 prior to heat sealing the sample tubes.

3.3. Crystal growth

3.3.1. $[XeOTeF_5][AsF_6]$

Crystals of $[XeOTeF_5][AsF_6]$ were grown as thin yellow plates over a period of several months at room temperature by sublimation onto the walls of a $\frac{1}{4}$ in. o.d. FEP tube pressurized to 1 atm with dry nitrogen. Suitable crystals of $[XeOTeF_5][AsF_6]$ were mounted inside the drybox equipped with a microscope, and sealed inside Lindemann glass capillaries. The crystal used for the X-ray structure determination had the dimensions $0.6 \times 0.3 \times 0.02$ mm^3.

3.3.2. $[XeOSeF_5][AsF_6]$

In the drybox, $[XeOSeF_5][AsF_6]$ (ca. 0.2 g) was loaded into a previously dried 40 cm long, 10 mm o.d. glass vessel joined to a metal valve by means of a graded glass/metal seal. The glass vessel was connected to a vacuum line, pressurized to 10 Torr with dry nitrogen, flame sealed, and then mounted at a 45° angle inside a fumehood. Clear, yellow crystals sublimed slowly onto the walls of the glass vessel over a period of several months. The crystals were freed from the walls of the vessel by mechanical shocking and mounted as described above. The crystal used for the X-ray structure determination had the dimensions $0.15 \times 0.08 \times 0.02$ mm^3.

3.3.3. $Xe(OTeF_5)_2$ and $Xe(OSeF_5)_2$

In the drybox, $Xe(OChF_5)_2$ (ca. 0.1 g; values in { } denote the selenium compound) was loaded into one arm of a T-shaped FEP reactor constructed from $\frac{1}{4}$ in. o.d. FEP tubing and fitted with a Kel-F valve. The reactor was attached to a glass vacuum line and Freon-114 was condensed onto $Xe(OChF_5)_2$. The reactor was then pressurized to 1 atm with dry nitrogen at −78°C and the solid was allowed to dissolve. The valved arm containing the solution mixture was attached to a glass vacuum line and placed inside a glass dewar adjusted to −18°C by means of a cold stream of dry nitrogen. The tube was then cooled slowly over a period of 4 {3} h to −30 {−10}°C. At −30 {−10}°C clear, colorless plates formed throughout the solution and along the walls of the tube. The tube was maintained at −30 {10}°C for an additional hour, and then the supernatant was decanted into the empty side arm of the reactor. The contents of the side arm were then frozen and separated from the apparatus using a heat seal. The tube containing the crystals was pressurized to 1 atm with dry nitrogen and maintained at −78 {0}°C. The crystal used for the data acquisition was mounted and heat sealed inside a glass Lindeman capillary and had the dimensions $0.25 \times 0.20 \times 0.06$ mm^3 {$0.30 \times 0.25 \times 0.20$ mm^3}.

Following data collection at −45°C, the $Xe(OSeF_5)_2$ crystal was shown to undergo a phase transition upon cooling to −79 (±2)°C, where a large number of additional diffraction spots appeared and the crystal ultimately powdered.

3.4. X-ray structure determinations

3.4.1. Collection and reduction of X-ray data

The crystals were centered on a P4 Siemens diffractometer, equipped with a Siemens SMART 1 K charge-coupled

device (CCD) area detector (using the program SMART [51]) and a rotating anode using graphite monochromated Mo Kα radiation ($\lambda = 0.71073$ Å). The crystal-to-detector distance was 5.000 cm, and the data collections were carried out in a 512×512 pixel mode using 2×2 pixel binning. Processing was carried out by using the program SAINT [51], which applied Lorentz and polarization corrections to three-dimensionally integrated diffraction spots. The program SADABS [52] was used for the scaling of diffraction data, the application of a decay correction, and an empirical absorption correction based on redundant reflections.

3.4.2. Solution and refinement of the structures

The XPREP program [53] was used to confirm the unit cell dimensions and the crystal lattices. All solutions were obtained using direct methods, which located the positions of the heavy atoms. Successive difference Fourier syntheses revealed the general positions of all the oxygen and fluorine atoms, implying a four-fold disorder for $[XeOTeF_5][AsF_6]$ and $[XeOSeF_5][AsF_6]$, and a three-fold disorder for $Xe(OSeF_5)_2$. The disorders are, however, different. In $[XeOChF_5][AsF_6]$, each atom is disordered around one site, while in $Xe(OSeF_5)_2$, each atom is disordered around three sites, implying that each O atom is positionally disordered with two other F atoms. This gives rise to a better disorder model for the cation than for the neutral compound. In contrast, the structure of $Xe(OTeF_5)_2$ was ordered. The final refinements were obtained by introducing anisotropic parameters for all the atoms in the case of $Xe(OTeF_5)_2$ and for only the heavy atoms in the three other disordered structures; and by introducing extinction parameters and weighting factors recommended by the refinement program. In the final difference Fourier maps, the maximum/minimum electron densities were located around the heavy atoms.[2]

3.5. Nuclear magnetic resonance

The NMR spectra of $[XeOSeF_5][AsF_6]$ in BrF_5 and neat SbF_5 solvents were recorded unlocked (field drift <0.1 Hz h^{-1}) on a Bruker AM 500 spectrometer [11.7440 T; ^{19}F (470.599 MHz), ^{77}Se (95.3838 MHz)] and on a Bruker WM 250 spectrometer [5.8719 T; ^{129}Xe (69.5626 MHz)] using 10 mm broad band probes for ^{77}Se and ^{129}Xe and a 5 mm probe for ^{19}F. The ^{19}F spectra were acquired in 16 (SbF_5) and 32 (BrF_5) K memories with spectral width settings of 20 kHz, yielding acquisition times of 0.410 (SbF_5) and 0.819 (BrF_5) s with data point resolutions of 2.44 (SbF_5) and 1.22 (BrF_5) Hz/data point; a pulse width of 1.00 μs was used. The ^{77}Se spectrum was acquired in a 16 K memory with a spectral width setting of 20 kHz, yielding an acquisition time of 0.410 s and data point resolution of 2.44 Hz/data point; a pulse width of 6.00 μs was used. The ^{129}Xe NMR spectra were acquired in 16 K memories with spectral width settings of 25 (SbF_5) and 20 (BrF_5) kHz, yielding acquisition times of 0.328 (SbF_5) and 0.410 (BrF_5) s and data point resolutions of 3.05 (SbF_5) and 2.44 (BrF_5) Hz/data point; a pulse width of 35.0 μs was used. Chemical shifts were referenced externally at 30°C with respect to neat samples of $CFCl_3$ (^{19}F), $XeOF_4$ (^{129}Xe) and $(CH_3)_2Se$ (^{77}Se).

3.6. Raman spectroscopy

The Raman spectra of $[XeOTeF_5][AsF_6]$ and $[XeOSeF_5][AsF_6]$ were recorded at −145°C on a Bruker RFS 100 FT Raman spectrometer equipped with a quartz beam splitter, a liquid nitrogen-cooled Ge diode detector, and a low-temperature accessory. The backscattered (180°C) radiation was sampled. The scanner velocity was 5 kHz, and the wavelength range for acquisition was 5500–10,500 cm^{-1} when shifted relative to the laser line at 9394 cm^{-1}, giving a spectral range of 3895 to −1105 cm^{-1}. The actual usable Stokes range was 50–3500 cm^{-1} with a spectral resolution of 2 cm^{-1}. The Fourier transformations were carried out by using a Blackman Harris three-term apodization and a zero-filling factor of 4. The 1064 nm line of an Nd YAG laser (350 mW maximum output) was used for excitation of the sample with a laser spot of ca. 0.2 mm at the sample. The spectra were recorded at −145°C on powdered microcrystalline samples, which were sealed under ca. 1 atm of dry N_2 inside Pyrex melting point capillaries, using laser powers of 200 {178} mW and averaged over 500 {200} scans (values for $[XeOTeF_5][AsF_6]$ are not bracketed and those for $[XeOTeF_5][AsF_6]$ are given in brackets { }).

3.7. Calculations

The calculations were done at the DFT and HF levels. The DFT calculations were done with the program DGauss [54–57] on an SGI computer system. The DZVP2 basis set [58] was used for H, N, O and F. For Te and Xe, a basis set was used in which the Kr core electrons were treated with a pseudopotential (PP) [59,60] and the remaining electrons were treated with a polarized valence double-ζ basis set. For Se, a PP basis set was used for the Ar core electrons. The calculations were done at the local level with the potential fit of Vosko et al. [61]. The geometries were optimized by use of analytic gradient methods and second derivatives were also calculated analytically. For the NBO analysis [62–66] at the DFT level, the NBO program integrated with Gaussian-98 was used [43]. For the NBO calculations, the polarized valence double-ζ basis set of Dunning and Hay [44] was used for O and F, and an all-electron basis set from Huzinaga et al. [45] contracted to valence polarized double-ζ was used

[2] Crystallographic data for the structures in this paper have been deposited with the Fachinformationzentrum Karlsruhe (FIZ) as supplementary publication Nos. CSD 411809, CSD 411810, CSD 411811 and CSD 411812. Copies of the data can be obtained, free of charge, on application to FIZ, abt. PROKA, 76344 Eggenstein–Leopoldshafen, Germany (Tel.: +49-7247-808-205 or e-mail: crysdata@fiz-karlsruhe.de).

for Te and Xe. The HF calculations were done with the program Gaussian-98 [43]. For O and F, a polarized valence double-ζ basis set was used [44] and for As, an all-electron basis set from Huzinaga et al. [45] was used. For Te and Xe, a polarized double-ζ valence basis set was used with an effective core potential [67–69].

4. Conclusion

The present study describes the first synthesis and characterization of the $XeOSeF_5^+$ cation and significantly extends the X-ray crystallographic data for Xe(II) derivatives of the $OSeF_5$ and $OTeF_5$ groups. The structures of the $XeOSeF_5^+$ and $XeOTeF_5^+$ cations as well as that of $Xe(OTeF_5)_2$ are described for the first time and that of $Xe(OSeF_5)_2$ has been redetermined at low temperature in a different space group, providing an improved refinement of that structure. Electronic structure calculations reveal that the geometric parameters in the gas phase, including the dihedral angles in $Xe(OChF_5)_2$, are in good agreement with experiment. The calculated vibrational frequencies corresponding to the energy minimized geometries have provided full assignments of the vibrational spectra of $XeOChF_5^+$ and $Xe(OChF_5)_2$ and have led to the reassignment of a number of frequencies previously reported for $XeOTeF_5^+$, $Xe(OSeF_5)_2$ and $Xe(OTeF_5)_2$. A comparison of the ^{129}Xe NMR chemical shifts for $XeOChF_5^+$ under similar solvent and temperature conditions show the same chemical shift trend as $Xe(OChF_5)_2$, and are in accord with a higher electronegativity for the $OSeF_5$ group than for the $OTeF_5$ group.

Acknowledgements

We thank the donors of the Petroleum Research Fund, administered by the American Chemical Society, for support of this work under ACS-PRF No. 33594-AC3. The density functional theory calculations were performed in the William R. Wiley Environmental Molecular Sciences Laboratory under the auspices of the Office of Basic Energy Sciences, US Department of Energy under Contract DE-ACO6-76RL0 1830 with the Battelle Memorial Institute, which operates the Pacific Northwest National Laboratory, a multiprogram national laboratory operated for the Department of Energy.

References

[1] D. Lentz, K. Seppelt, Angew. Chem. 390 (1978) 390–391; Angew. Chem. Int. Ed. Engl. 17 (1978) 355–356.
[2] P. Huppmann, D. Lentz, K. Seppelt, Z. Anorg. Allg. Chem. 472 (1981) 26–32.
[3] T. Birchall, R.D. Myers, H. Waard, G.J. Schrobilgen, Inorg. Chem. 21 (1982) 1068–1073.
[4] K. Seppelt, Acc. Chem. Res. 12 (1979) 211–216.
[5] K. Seppelt, Angew. Chem. 94 (1982) 890–901; Angew. Chem. Int. Ed. Engl. 21 (1982) 877–888.
[6] K. Seppelt, D. Lentz, G. Klöter, in: Inorganic Syntheses, Vol. 24, Wiley, New York, 1986, pp. 27–31.
[7] F. Sladky, Monatsh. Chem. 101 (1970) 1578–1582.
[8] N. Keller, G.J. Schrobilgen, Inorg. Chem. 20 (1981) 2118–2129.
[9] K. Seppelt, H.H. Rupp, Z. Anorg. Allg. Chem. 409 (1974) 338–342.
[10] R.C. Burns, L.A. Devereux, P. Granger, G.J. Schrobilgen, Inorg. Chem. 24 (1985) 2615–2624.
[11] M. Björgvinsson, J.F. Sawyer, G.J. Schrobilgen, Inorg. Chem. 26 (1987) 741–749.
[12] R.J. Gillespie, G.J. Schrobilgen, Inorg. Chem. 13 (1974) 1230–1235.
[13] L.K. Templeton, D.H. Templeton, K. Seppelt, N. Bartlett, Inorg. Chem. 15 (1976) 2718–2720.
[14] F. Sladky, Monatsh. Chem. 101 (1970) 1559–1570.
[15] L. Pauling, The Nature of the Chemical Bond, 3rd Edition, Cornell University Press, Ithaca, New York, 1960, p. 260.
[16] A. Bondi, J. Phys. Chem. 68 (1964) 441–451.
[17] A. Zalkin, D.L. Ward, R.N. Biagioni, D.H. Templeton, N. Bartlett, Inorg. Chem. 17 (1978) 1318–1322.
[18] J.M. Whalen, B.A. Fir, H.P.A. Mercier, D.A. Dixon, G.J. Schrobilgen, Inorg. Chem., submitted for publication.
[19] J. Burgess, C.J.W. Fraser, V.M. McRae, R.D. Peacock, D.R. Russell, J. Inorg. Nucl. Chem. (Suppl.) (1976) 183–188.
[20] P.A. Argon, G.M. Begun, H.A. Levy, A.A. Mason, C.G. Jones, D.F. Smith, Science 139 (1963) 842–844.
[21] N. Bartlett, M. Wechsberg, G.R. Jones, R.D. Burbank, Inorg. Chem. 11 (1972) 1124–1127.
[22] L. Turowsky, K. Seppelt, Inorg. Chem. 29 (1990) 3226–3228.
[23] J.F. Lehmann, D.A. Dixon, G.J. Schrobilgen, Inorg. Chem. 40 (2001) 3002–3017.
[24] H. Oberhammer, K. Seppelt, Inorg. Chem. 17 (1978) 1435–1439.
[25] P. Zylka, H. Oberhammer, K. Seppelt, J. Mol. Struct. 243 (1991) 411–418.
[26] H.P.A. Mercier, J.C.P. Sanders, G.J. Schrobilgen, J. Am. Chem. Soc. 116 (1994) 2921–2937.
[27] H.P.A. Mercier, J.C.P. Sanders, G.J. Schrobilgen, Inorg. Chem. 34 (1995) 5261–5273.
[28] W.J. Casteel Jr., D.M. MacLeod, H.P.A. Mercier, G.J. Schrobilgen, Inorg. Chem. 35 (1996) 7279–7288.
[29] R.J. Gillespie, I. Hargittai, The VSEPR Model of Molecular Geometry, Allyn & Bacon, Boston, 1991.
[30] L. Turowsky, K. Seppelt, Z. Anorg. Allg. Chem. 609 (1992) 153–156.
[31] R.J. Gillespie, G.J. Schrobilgen, Inorg. Chem. 15 (1976) 22–31.
[32] R. Faggiani, D.K. Kennepohl, C.J.L. Lock, G.J. Schrobilgen, Inorg. Chem. 25 (1986) 563–571.
[33] G.J. Schrobilgen, J.M. Whalen, Inorg. Chem. 33 (1994) 5207–5218.
[34] K. Seppelt, Z. Anorg. Allg. Chem. 399 (1973) 87–96.
[35] G. Gundersen, K. Hedberg, T.G. Strand, J. Chem. Phys. 68 (1978) 3548–3552.
[36] V.C. Ewing, L.E. Sutton, Trans. Faraday Soc. 59 (1963) 1241.
[37] Y.M. Bosworth, R.G.H. Clark, D.M. Rippon, J. Mol. Spectrosc. 46 (1973) 240–255.
[38] H.H. Claassen, G.L. Goodman, J.H. Holloway, H. Selig, J. Chem. Phys. 53 (1970) 341–348.
[39] I. Mayer, Chem. Phys. Lett. 97 (1983) 270–274.
[40] I. Mayer, Theor. Chim. Acta 67 (1985) 315–322.
[41] I. Mayer, Int. J. Quantum Chem. 29 (1986) 73–84.
[42] I. Mayer, Int. J. Quantum Chem. 29 (1986) 477–483.
[43] M.J. Frisch, G.W. Trucks, H.B. Schlegel, G.E. Scuseria, M.A. Robb, J.R. Cheeseman, V.G. Zakrzewski, G.A. Petersson, J.A. Montgomery Jr., R.E. Stratmann, J.C. Burant, S. Dapprich, J.M. Millam, A.D. Daniels, K.N. Kudin, M.C. Strain, O. Farkas, J. Tomasi, V. Barone, M. Cossi, R. Cammi, B. Mennucci, C. Pomelli, C. Adamo, S. Clifford, J. Ochterski, G.A. Petersson, P.Y. Ayala, Q. Cui, K. Morokuma, D.K. Malick, A.D. Rabuck, K. Raghavachari, J.B.

Foresman, J. Cioslowski, J.V. Ortiz, B.B. Stefanov, G. Liu, A. Liashenko, P. Piskorz, I. Komaroni, R. Gomperts, R.L. Martin, D.J. Fox, T.A. Keith, M.A. Al-Laham, C.Y. Peng, A. Nanayakkara, C. Gonzalez, M. Challacombe, P.M.W. Gill, B.G. Johnson, W. Chen, M.W. Wong, J.L. Andreas, M. Head-Gordon, E.S. Replogle, J.A. Pople (Eds.), Gaussian-98, A.7, Gaussian Inc., Pittsburgh, PA, 1998.

[44] T.H. Dunning Jr., P.J. Hay, in: H.F. Schaefer III (Ed.), Methods of Electronic Structure Theory, Plenum Press, New York, 1977, pp. 1–27.

[45] S. Huzinaga, J. Andzelm, M. Klobukowski, E. Radio-Andzelm, Y. Sakai, H. Tatekawi, Gaussian Basis Sets for Molecular Calculations, Physical Sciences Data 16, Elsevier, Amsterdam, 1984.

[46] W.J. Casteel Jr., P. Kolb, N. LeBlond, H.P.A. Mercier, G.J. Schrobilgen, Inorg. Chem. 35 (1996) 929–942.

[47] H.P.A. Mercier, J.C.P. Sanders, G.J. Schrobilgen, S.S. Tsai, Inorg. Chem. 32 (1993) 386–393.

[48] R.J. Gillespie, A. Netzer, G.J. Schrobilgen, Inorg. Chem. 13 (1974) 1455–1459.

[49] A.A.A. Emara, G.J. Schrobilgen, Inorg. Chem. 31 (1992) 1323–1332.

[50] K.O. Christe, E.C. Curtis, D.A. Dixon, H.P.A. Mercier, J.C.P. Sanders, G.J. Schrobilgen, J. Am. Chem. Soc. 113 (1991) 3351–3361.

[51] SMART and SAINT, Release 4.05, Siemens Energy and Automation Inc., Madison, WI, 1994.

[52] G.M. Sheldrick, Siemens Area Detector Absorption Corrections (SADABS), Personal communication, 1996.

[53] G.M. Sheldrick, SHELXTL-Plus, Release 5.03, Siemens Analytical X-Ray Instruments Inc., Madison, WI, 1994.

[54] J.W. Andzelm, E. Wimmer, D.R. Salahub, in: D.R. Salahub, M.C. Zerner (Eds.), The Challenge of d and f Electrons: Theory and Computation, ACS Symposium Series, Vol. 394, American Chemical Society, Washington, DC, 1989, p. 228.

[55] J.W. Andzelm, in: J.K. Labanowski, J.W. Andzelm (Eds.), Density Functional Methods in Chemistry, Springer, New York, 1991, pp. 155–174.

[56] J.W. Andzelm, E. Wimmer, J. Chem. Phys. 96 (1992) 1280–1303.

[57] DGauss is a density functional program which is part of Unichem and is available from Oxford Molecular, San Diego, CA. Versions 4.1 and 5.0 Beta were used.

[58] N. Godbout, D.R. Salahub, J.W. Andzelm, E. Wimmer, Can. J. Chem. 70 (1992) 560–571.

[59] H. Chen, M. Krasowski, G. Fitzgerald, J. Chem. Phys. 98 (1993) 8710–8717.

[60] N. Troullier, J.L. Martins, Phys. Rev. B: Condens. Matter. 43 (1991) 1993–2006.

[61] S.H. Vosko, L. Wilk, M. Nusair, Can. J. Phys. 58 (1980) 1200–1211.

[62] A.E. Reed, L.A. Curtiss, F. Weinhold, Chem. Rev. 88 (1988) 899–926.

[63] J.P. Foster, F. Weinhold, J. Am. Chem. Soc. 102 (1980) 7211–7218.

[64] A.E. Reed, F. Weinhold, J. Chem. Phys. 78 (1983) 4066–4073.

[65] A.E. Reed, R.B. Weinstock, F. Weinhold, J. Chem. Phys. 83 (1985) 735–746.

[66] A.E. Reed, F. Weinhold, J. Chem. Phys. 83 (1985) 1736–1740.

[67] P.J. Hay, W.R. Wadt, J. Chem. Phys. 82 (1985) 270–283.

[68] P.J. Hay, W.R. Wadt, J. Chem. Phys. 82 (1985) 284–298.

[69] P.J. Hay, W.R. Wadt, J. Chem. Phys. 82 (1985) 299–310.